

Bond University
Research Repository



Structural behaviour of hardwood veneer-based circular hollow sections of different compactness

Gilbert, Benoit P.; Underhill, Ian D.; Fernando, Dilum; Bailleres, Henri; Miller, Dane

Published in:
Construction and Building Materials

DOI:
[10.1016/j.conbuildmat.2018.03.105](https://doi.org/10.1016/j.conbuildmat.2018.03.105)

Licence:
CC BY-NC-ND

[Link to output in Bond University research repository.](#)

Recommended citation(APA):
Gilbert, B. P., Underhill, I. D., Fernando, D., Bailleres, H., & Miller, D. (2018). Structural behaviour of hardwood veneer-based circular hollow sections of different compactness. *Construction and Building Materials*, 170, 557-569. <https://doi.org/10.1016/j.conbuildmat.2018.03.105>

General rights

Copyright and moral rights for the publications made accessible in the public portal are retained by the authors and/or other copyright owners and it is a condition of accessing publications that users recognise and abide by the legal requirements associated with these rights.

For more information, or if you believe that this document breaches copyright, please contact the Bond University research repository coordinator.

1 **STRUCTURAL BEHAVIOUR OF HARDWOOD VENEER-BASED CIRCULAR HOLLOW**
2 **SECTIONS OF DIFFERENT COMPACTNESS**

3 Benoit P. Gilbert⁽¹⁾, Ian D. Underhill⁽¹⁾, Dilum Fernando⁽²⁾, Henri Bailleres⁽³⁾, Dane Miller⁽⁴⁾

4 ⁽¹⁾ School of Engineering and Built Environment, Griffith University, Australia

5 ⁽²⁾ School of Civil Engineering, The University of Queensland, Australia

6 ⁽³⁾ Salisbury Research Facility, Department of Agriculture and Fisheries, Queensland Government, Australia

7 ⁽⁴⁾ Faculty of Society & Design, Bond University, Australia

8 Corresponding author: b.gilbert@griffith.edu.au

9
10 **Abstract:** This paper presents the capacity and structural behaviour of hardwood veneer-based cir-
11 cular hollow sections (CHS) tested in bending, shear and compression. The sections were manufac-
12 tured from early to mid-rotation (juvenile) Gympie messmate (*Eucalyptus cloeziana*) plantation
13 thinned logs. In total twenty-one 167 mm Outside Diameter (OD) \times 1.2 m long CHS were manufac-
14 tured in seven sets of three nominally identical sections. Two different wall thicknesses were inves-
15 tigated to produce nine compact and twelve more slender cross-sections. The sections were also man-
16 ufactured in three different structural grades. A sudden failure mode was observed in the compression
17 zone of the slender sections tested in bending. In compression, the compact sections showed a ductile
18 behaviour, while the slender sections showed a more brittle behaviour, with the sections bursting into
19 longitudinal strips. While a relationship was observed between the bending and compressive capaci-
20 ties, and the structural grade, no such relationship was noticed for the shear capacity. Comparison to
21 steel and concrete sections of similar outside diameter proved that the timber sections are the most
22 efficient in terms of bending and compressive capacity to linear weight ratio. The timber sections fall
23 behind their steel and concrete counterparts in terms of shear efficiency, however they still have
24 enough shear capacity for representative structural applications.

25

26 **1. INTRODUCTION**

27 To develop a market for low-value, small diameter, early to mid-rotation (juvenile) hardwood
28 plantation logs, veneer-based hollow sections are currently being developed in Australia [1-3], see
29 Figure 1. These sections have the potential to be used in structural applications [1, 3] and are seen,
30 for instance, as a potential solution for utility poles [1] and the main frame of buildings. They have
31 the advantage of having an efficient cross-sectional shape, are sustainable [4-6], and able to be man-
32 ufactured in usable lengths [2] and cross-sectional sizes that are no longer available in sawn timber.

33 In the literature, various hollow timber structural solutions have been investigated. They include
34 (i) spirally winded veneer-based Circular Hollow Section (CHS) [7-9], (ii) fibre-reinforced moulded
35 wooden tubes [10-14], (iii) octagonal tubes from composite wood flakes panels [15], (iv) nonagon
36 tubes from knot free pine wood strips [16], (v) “wood rings” reinforced with glass epoxy [17] and
37 (vi) LVL type CHS for temporary geotechnical soil nailing systems [18]. Commercially, veneer-
38 based hollow timber solutions are also available, either limited to small diameter cross-sections (up
39 100 mm) [19] or short lengths (up to 1,000 mm) [20].

40 To confidently use the new sections in structural applications, research is still needed to fully un-
41 derstand their structural behaviour, failure modes and reliability. In particular, bending tests per-
42 formed on 145 mm Outside Diameter (OD) \times 15 mm (wall thickness) Laminated Veneer Lumber
43 (LVL) type CHS showed that the sections can experience a sudden failure in the compression zone,
44 with the sections opening up [1]. While this failure mode has been observed in hollow trees [21], it
45 is not typical of solid timber beams which usually reach a maximum bending moment due to tensile
46 rupture [22]. The sudden compressive failure mode is likely attributed to the semi-compactness of
47 the cross-section in [1] which led to local buckling and cross-section ovalisation (Brazier effect [23]).
48 The relationship between the cross-sectional slenderness and structural behaviour requires further
49 attention.

50 Consequently, the structural behaviour and failure modes of veneer-based timber CHS of various
51 cross-sectional slenderness are experimentally investigated in bending, shear and compression in this
52 paper. In total twelve 167 mm (OD) \times 12.5 mm (wall thickness), referred to as “slender”, and nine
53 167 mm (OD) \times 25 mm (wall thickness), referred to as “compact”, 1.2 m long CHS were manufac-
54 tured from early to mid-rotation (juvenile) Gympie messmate (*Eucalyptus cloeziana*) plantation
55 thinned logs. The veneer grain was orientated in the same direction and along the member longitudi-
56 nal axis for all sections except for one type of the slender sections. For this section, cross-banded
57 veneers were used in this case to potentially increase the section local buckling capacity. To study
58 the effect of the timber elastic stiffness on the new products’ structural behaviour, the CHS were
59 manufactured in three different structural grades. The grades were solely based on the veneers’ Mod-
60 ulus of Elasticity (MOE).

61 The paper initially introduces the investigated cross-sections and the associated manufacturing
62 process. Secondly, the test set-ups for all investigated loading cases are presented. Thirdly, the struc-
63 tural behaviour, capacities and failure modes of the slender and compact sections are analysed and
64 discussed. Finally, the performance of the studied sections is compared to similar steel and concrete
65 counterparts.

66

67 **2. INVESTIGATED CROSS-SECTIONS**

68 **2.1 General**

69 In total, twenty-one nominal 167 mm (OD) \times 1.2 m long veneer-based CHS were manufactured
70 from two half cross-sections following the process described later in Section 2.2. Randomly selected
71 nominal 1.2 m (Long) \times 1.2 m (Wide) \times 2.5 mm (Thick) Gympie messmate rotary peeled veneer
72 sheets were delivered and then cut parallel to the grain direction (i.e. perpendicular to the length of
73 the veneer ribbon) into four 300 mm wide strips. The longitudinal dynamic MOE of each veneer sheet

74 was then measured using a non-destructive resonance method [24]. To do so, the second cut strip per
75 veneer sheet was simply supported on rubber bands and impacted with a hammer in its longitudinal
76 direction. The sample natural frequency was recorded using a microphone and analysed using the
77 software BING[®] (Beam Identification by Non-destructive Grading) [25]. Figure 2 shows a photo of
78 the set-up. Before assessing the dynamic MOE, the veneers were conditioned in a temperature con-
79 trolled room set at 22°C.

80 Based on their measured MOE, the delivered veneer sheets were divided into three stacks of equal
81 number of veneers. This classified the veneers into three grades referred to as “Grade 1” for the lower
82 MOE ($13 \text{ GPa} < \text{MOE} \leq 19 \text{ GPa}$), “Grade 2” for the intermediate MOE ($19 \text{ GPa} < \text{MOE} \leq 21 \text{ GPa}$)
83 and “Grade 3” for the higher MOE ($21 \text{ GPa} < \text{MOE} \leq 25 \text{ GPa}$).

84 The twenty-one CHS were manufactured in seven sets of three nominal identical samples. Per set,
85 the half cross-sections of the three nominally identical CHS were manufactured from the same veneer
86 sheets which were glued in the exact same order. Precisely, for each veneer sheet, three 300 mm wide
87 strips out of four were used in the CHS manufacturing process. The remaining strip was used to
88 determine the material properties of the half cross-sections as detailed in Sections 2.2 and 3.2. The
89 seven sets consisted of:

- 90 • Three sets of nominal 167 mm (OD) \times 12.5 mm (5-ply) slender CHS manufactured from Grade 1
91 (Set “S_G1”), Grade 2 (Set “S_G2”) and Grade 3 (Set “S_G3”) veneers. In these sets, the veneers’
92 grain is orientated in the same direction and along the longitudinal axis of the section.
- 93 • One set of nominal 167 mm (OD) \times 13 mm slender CHS. To potentially increase the section local
94 buckling capacity, a cross-banded configuration was used. Four 2.5 mm thick Gympie messmate
95 hardwood Grade 2 veneers were orientated along the longitudinal axis of the section and three 1
96 mm thick cross-banded softwood Hoop pine (*Araucaria cunninghamii*) veneers were inserted be-
97 tween the hardwood veneers to form a 7-ply configuration. This set is referred to as “S_G2_Cross”.

98 • Three sets of nominal 167 mm (OD) × 25 mm (10-ply) compact CHS manufactured from Grade 1
99 (Set “C_G1”), Grade 2 (Set “C_G2”) and Grade 3 (Set “C_G3”) veneers. In these sets, the veneers’
100 grain is orientated in the same direction and along the longitudinal axis of the section.

101 An examples of a compact and slender CHS is shown in Figure 1 (a).

102 Note that while the wall the slender sections is quite thin, fire protection may be achieved by gluing
103 sacrificial low MOE veneers to the outside of the sections, therefore protecting the load carrying part
104 of the CHS.

105 **2.2 Manufacturing process**

106 The manufacturing process detailed in [18, 26] and used to manufacture the samples tested in [1,
107 2] has been improved in this study. A similar process to the one described in [18, 27] has been fol-
108 lowed. After assessing the dynamic MOE of the veneers, the veneers were moved out of the temper-
109 ature controlled room and stored in an indoor environment (structure laboratory) until gluing. To form
110 the half cross-sections, resorcinol formaldehyde structural adhesive was applied to the veneer strips
111 at ambient temperature and humidity. The veneer stacks were then inserted into a 167 mm Internal
112 Diameter (ID) CHS PVC pipe and cold-pressed for 24 hours by a fire hose inserted into the PVC pipe
113 and pressurised at 1.2 MPa with water. Figure 3 illustrates the manufacturing process.

114 As rotary peeled veneers have the natural tendency to curl about their loose side (i.e. the one in
115 contact with the blade of the peeling lathe), the loose side of a veneer was always glued herein to the
116 tight side of the next veneer. The tight and loose veneer sides therefore formed the outside and inner
117 faces of the manufactured hollow cross-sections, respectively. The two half cross-sections forming a
118 complete CHS were then butt jointed together using structural epoxy resin (Figure 1 (b)) due to its
119 good gap properties which can compensate for non-strict parallelism of the two half cross-sections.
120 For alignment, the glue-line incorporated biscuit joints every 400 mm.

121 Additionally, to determine the mechanical properties of the material of the timber sections, two
122 500 mm × 300 mm flat panels were also manufactured for each half-section. The panels were manu-
123 factured from the same veneer sheets used to produce the half cross-sections and were glued in the
124 exact same layering order.

125

126 **3. TESTING METHODOLOGY**

127 **3.1 General**

128 Per manufactured set, one section was tested in bending, one in shear and one in compression. The
129 following sub-sections introduce the material testing methodology and the test set-ups of the CHS for
130 each one of the investigated loading cases.

131 Before testing, all samples were conditioned in the same temperature controlled room as the ve-
132 neers when the dynamic MOE was assessed, for a minimum period of one month. The temperature
133 in the room was set at 22°C. For all scenarios, excluding the CHS tested in compression, pieces were
134 cut and weighed immediately after testing from selected test samples to determine the timber moisture
135 content at the time of testing. The oven-dry methodology in the Australian and New Zealand standard
136 AS/NZS 1080.1 [28] was followed.

137 **3.2 Material properties**

138 **3.2.1 Tension tests**

139 From the first flat panel of each half cross-section, a maximum of five nominal 10 mm wide × 100
140 mm long (gauge length) coupon (dog bone) samples were CNC cut. The samples were similar to the
141 ones recommended by the ASTM D3500–14 [29] and were used to estimate the tensile strength of
142 each half cross-section. The ends of the samples were clamped in the jaws of a 500 kN capacity MTS
143 universal testing machine and tested in tension at a constant strain rate to reach failure in 3-6 mins.

144 The tensile strength σ_{tens} of each coupon was calculated as,

145

$$\sigma_{tens} = \frac{F_{max}}{W_t t_t} \quad (1)$$

146 where F_{max} is the maximum recorded force, W_t and t_t are the measured width and thickness of the
147 coupons, respectively.

148 3.2.2 Compression tests

149 The second flat panel of each half cross-section was used to determine the compressive strength
150 of the material. To avoid buckling of the samples corresponding to the slender CHS, the 12.5 mm
151 thick panels were cut in two and glued together using resorcinol formaldehyde structural adhesive to
152 form nominal 25 mm thick panels. The panels corresponding to the compact CHS were left un-
153 touched. Up to four 80 mm (Wide) \times 150 mm (Long) rectangular samples were cut per panel for
154 material testing.

155 The samples were tested in compression in a 500 kN capacity MTS universal testing machine at a
156 constant strain rate to reach the peak stress in 3-5 mins. Specifically, the samples were positioned
157 between a fixed bottom platen and an upper platen mounted on a spherical seat, which could rotate,
158 so as to provide full contact between the platens and the specimens. Note that before testing, the ends
159 of the samples were cut with a high quality fine cut circular saw blade to ensure a uniform contact
160 pressure between the platens and the samples.

161 Similar to Eq. (1), the compressive strength σ_{comp} of each sample was calculated as,

162

$$\sigma_{comp} = \frac{F_{max}}{W_c t_c} \quad (2)$$

163 where F_{max} is the maximum recorded force, W_c and t_c are the measured width and thickness of the
164 samples, respectively.

165

166 3.3 *Bending tests*

167 3.3.1 *Test set-up*

168 To measure the bending strength and stiffness of the timber CHS, the sections were tested in a
169 similar manner to the one reported in [2]. A pair of four reinforced quarter steel tubes, 240 mm long,
170 were designed and manufactured to rigidly clamp each end of the CHS, as shown in Figure 4. Each
171 steel clamp was bolted to a steel Rectangular Hollow Section (RHS) to form a 2,360 mm long beam.
172 To avoid local crushing of the timber CHS and fully transfer the moment from the steel RHS to the
173 timber with minimum stress concentration, two part epoxy resin was poured at the steel-timber con-
174 nection (i) in the inside of the timber CHS filled with plywood and (ii) on the outside of the timber
175 CHS to match the inside diameter of the four quarter steel tubes. On top of the friction forces applied
176 by the clamps to the timber, screws connecting the steel to the timber were also added to further
177 prevent sliding of the timber sections in the clamps. The overall test set-up is shown in Figure 5.

178 The sections were then tested in a 500 kN capacity MTS universal testing machine, with the load
179 being applied to the steel RHS, as shown in Figure 5. The tests were run in displacement control and
180 reached failure in 3-4 minutes for the slender sections and 5-6 minutes for the compact sections. For
181 all tests, the butt joints between two half-sections lied in the horizontal plane.

182 Three Laser Displacement Sensors (LDS) recorded the vertical displacement at the bottom fibre
183 of the timber sections for simplicity in the test set-up. Additionally, two 30 mm strain gauges (SG)
184 recorded the mid-span longitudinal strain at the top (compression) and bottom (tension) fibres of the
185 timber CHS. A third 30 mm strain gauge recorded the mid-span tangential stress to better apprehend
186 the cross-sectional deformation. Locations and numbering of all LDS and strain gauges are given in
187 Figure 5 (b). The 300 mm distance between LDS was chosen so the edge LDS are away for the
188 clamping ends while placing the LDS the further away from each other.

189 3.3.2 *Evaluations*

190 The applied moment M to the hollow timber sections is calculated as,

191
$$M = \frac{(F + F_w)L_1}{2} \quad (3)$$

192 where F is the total applied load, $F_w = 2.37$ kN is the gravity load applied by the steel rig (including
 193 the steel CHS and measured at the points of application of the load) and $L_1 = 455$ mm is given in
 194 Figure 5 (b). The bending capacity M_b is defined as the maximum applied moment M and the bending
 195 strength f_b is obtained from the well-known equation,

196
$$f_b = \frac{M_b}{Z} \quad (4)$$

197 where Z is the section modulus calculated from the measured cross-sectional dimensions, assuming
 198 a perfect composite action between the two half cross-sections.

199 The relative displacement δ of the timber sections is calculated from the displacements δ_1 , δ_2 and
 200 δ_3 recorded by the LDS number 1, 2 and 3, respectively, as,

201
$$\delta = \delta_1 - \frac{\delta_2 + \delta_3}{2} \quad (5)$$

202 The static MOE E_s parallel to the grain of the timber sections is calculated from the bending stiff-
 203 ness $E_s I_s$ defined as,

204
$$E_s I_s = \frac{k_t d^2}{2} \quad (6)$$

205 where I_s is the second moment of area of the CHS (calculated from measured dimensions), d is given
 206 in Figure 5 (b) and k_t is the stiffness of the linear part of the experimental moment-displacement curve
 207 ($M-\delta$), calculated by performing a linear regression between 5 kN.m and 20 kN.m for the compact
 208 sections and 2.5 kN.m and 15 kN.m for the slender ones. Note that Eq. (6) assumes that the relative
 209 displacement δ is measured at the neutral axis. Yet, using the relative displacement measured in this
 210 study at the bottom fibre of the section provides accurate results, with a maximum error in determin-
 211 ing $E_s I_s$ of less than 0.5%.

212 3.4 Shear tests

213 3.4.1 Test set-up

214 To estimate the shear strength of the timber CHS, the sections were tested in three point bending,
215 similarly to the tests performed in [1]. The sections were simply supported with a distance $L = 500$
216 mm between two consecutive loads, as shown in the schematic test set-up in Figure 6. To avoid local
217 crushing of the sections, two part epoxy resin (combined with plywood) was poured inside the CHS
218 at the load application point and supports. The butt joints between two half cross-sections lied in the
219 horizontal plane. For each set, the half cross-section which was in compression in the bending test
220 (Section 3.3) was also in compression in the shear test. The tests were performed in a 500 kN capacity
221 MTS universal testing machine in displacement control and reached failure in 6-8 minutes for all
222 sections but for S_G3 which was tested at a higher strain rate and reached failure in 2 minutes.

223 3.4.2 Evaluations

224 The shear strength f_s of the hollow timber sections is calculated using the shear area of a CHS as
225 [30],

$$226 \quad f_s = \frac{F_{\max}}{\frac{3}{2} A \left(\frac{R_o^2 + R_i^2}{R_o^2 + R_o R_i + R_i^2} \right)} \quad (7)$$

227 where F_{\max} is the total maximum applied load, A is the measured CHS cross-sectional area, and R_o
228 and R_i are the measured CHS external and internal radii, respectively. The shear capacity V_s is calcu-
229 lated as $F_{\max}/2$.

230 3.5 Compressive tests

231 3.5.1 Test set-up

232 To measure the compressive strength and stiffness of the timber CHS, the sections were tested in
233 compression in a 10 MN capacity MTS universal testing machine. The sections were positioned be-
234 tween a fixed bottom platen and an upper platen mounted on a spherical seat, which could rotate. The

235 samples were mechanically sanded flat in a milling machine before testing to ensure a uniform contact
236 pressure between the platens and the CHS. The tests were performed in displacement control and
237 reached failure in 3-4 minutes for the slender sections and 5-6 minutes for the compact sections. The
238 test set-up is shown in Figure 7.

239 Two diametrically opposed 30 mm strain gauges, glued parallel to the column axis, each located
240 in the middle of a half cross-section and 150 mm from the bottom end of the sections, recorded the
241 longitudinal deformation. Strain gauges numbering is given in Figure 7.

242 3.5.2 Evaluations

243 The compressive stress σ of the hollow timber sections is calculated as,

$$244 \quad \sigma = \frac{F}{A} \quad (8)$$

245 where F is the applied load and A is the measured CHS cross-sectional area. The compressive capacity
246 R_c and strength f_c are defined as the maximum applied force and compressive stress, respectively.

247 The static MOE E_s is calculated by performing a linear regression on the linear part of the stress-
248 strain curve (σ - ε) between 5 MPa and 40 MPa. The strain ε is calculated as the average of strains ε_1
249 and ε_2 from strain gauges 1 and 2, respectively.

250

251 4. RESULTS AND DISCUSSION

252 4.1 Material properties

253 Table 1 gives the tensile and compressive strengths of the material of each half cross-section of
254 each investigated set. As the veneer MOE increases with the grade, so typically does the measured
255 material strength [31]. For the LVL samples, the compressive strength ranges from 58.6 MPa (S_G1)
256 to 77.9 MPa (C_G3 and S_G3), and the tensile one from 96.3 MPa (C_G1) to 135.8 (C_G3). Due to
257 the nature of the brittle tensile failure mode compared to the ductile compressive failure mode of

258 timber samples, the Coefficients of Variation (CoV) of the tensile test results are typically higher than
259 the ones of the compressive test results. The average oven dry moisture content at the time of testing
260 of the tension and compression samples is reported in Table 2.

261 **4.2 Bending tests**

262 *4.2.1 Capacities and failure modes*

263 The bending capacities M_b and strengths f_b for all CHS tested in bending are reported in Table 3,
264 along with the measured static MOE E_s (Eq. (6)) and observed failure modes. Two of the slender
265 sections (S_G1 and S_G3) failed in buckling of the compression fibre, with the section opening up,
266 as shown in Figure 8 (a). Slender S_G2 and compact C_G1 sections failed in tensile rupture, as shown
267 in Figure 8 (b). The cross-banded CHS (C_G2_Cross) prematurely failed in the butt joint between
268 the two half cross-sections, as shown in Figure 8 (c). This weak zone was only observed for all testing
269 configurations in C_G2_Cross, as later reported in Sections 3.4 and 0. In all other sections and sec-
270 tions tested in [1, 2], failure never developed in the butt joint. For compact sections C_G2 and C_G3,
271 the steel clamps did not provide sufficient restraints and the sections ultimately slid at the steel-timber
272 connections, leading to shear failure, as shown in Figure 8 (d). However, the maximum bending
273 stresses reached for these two sections are higher than the bending strengths f_b of all other tested
274 sections. It is therefore very likely that the maximum recorded moments are within a few percent of
275 the bending capacities M_b of the sections. Noting that these maximum recorded moments represent
276 lower bound values of M_b , their values are conservatively taken for M_b herein for both C_G2 and
277 C_G3 sections. For all sections, the bending strength typically increases with the veneer MOE (or
278 grade).

279 The compact sections reached on average a bending strength f_b 18% higher than the one of the
280 slender sections of the same grade. This result is attributed to different material strengths between
281 sections (Table 1) and possibly to the section compactness. Indeed, when buckling develops in the
282 compression zone of the slender sections, it would result in a loss in stiffness of the section wall,

283 consequently inducing a shift of the neutral axis and a higher stress in the tension zone. The sections
284 would eventually fail in the compression zone (S_G1 and SG_G3) or tension zone (S_G2), whichever
285 zone is the weakest. Such phenomenon would not occur for compact sections for which the compres-
286 sive zone only experiences plasticity without buckling, as typically observed in timber beams [22]. A
287 similar tensile failure mode to the one experienced in timber beams would be therefore expected.

288 More investigations are needed to (i) fully comprehend the mechanisms involved in the observed
289 failure modes of the slender sections, (ii) validate the hypothesis in the above paragraph and (iii)
290 quantify the influence of the cross-sectional geometry, timber compressive and tensile strengths on
291 the full section capacity. Numerical models, similar to the one developed in [1], can be used to predict
292 the capacity of compact sections.

293 Note that the cross-banded section (S_G2_Cross) has a bending strength f_b and static MOE E_s 9%
294 and 55%, respectively, lower than the ones of the slender section of the same grade (S_G2). Cross-
295 banded veneer-based CHS would gain further structural optimisation, such as number and thickness
296 of the cross bands.

297 4.2.2 Behaviour

298 Figure 9 plots the Moment-Displacement curves ($M-\delta$) of all investigated sections. While a large
299 non-linear behaviour is observed for the compact sections, it is limited for the slender sections, except
300 for the cross-banded one. As outlined in Figure 9, when failure occurred the moment suddenly
301 dropped for all sections. This observed drop for the two slender sections failing in buckling of the
302 compression zone (S_G1 and S_G3) is due to the sections opening up.

303 Figure 10 (a) shows the readings of the two strain gauges glued in the section longitudinal axis
304 (SG 1 and SG 3). Timber elements loaded in tension typically exhibit a linear behaviour until fracture
305 suddenly occurs at the maximum tensile strength, and the strain recorded on the tension zone (SG 3)

306 is consequently almost linear. Plasticity occurred on the compression side (SG 1) at an applied mo-
307 ment of about 20-25 kN.m and 12-15 kN.m for the compact and slender sections, respectively. This
308 corresponds to bending stresses of about 60 MPa to 75 MPa, i.e. of the same order of magnitude of
309 the material compressive strengths reported in Table 1. Due to the buckling of the compression zone
310 for S_G1 and S_G3, reading of Strain gauge 2 reached a plateau for these sections at about 12,000 to
311 16,000 $\mu\epsilon$.

312 The transverse strain recorded by SG 2 is plotted in Figure 10 (b). The figure mainly indicates that
313 the transverse strain significantly increased when plasticity damage occurred in the compression zone.
314 The strain reversal experienced for S_G1 and S_G3 is likely attributed to the buckling and ovalisation
315 of the cross-sections.

316 The average oven dry moisture content at the time of testing of the sections tested in bending is
317 reported in Table 2.

318 **4.3 Shear tests**

319 Table 4 gives the experimental shear capacities V_s and strengths f_s for all investigated sections. All
320 sections failed in the timber except S_G2_Cross which failed in the butt joint between the two half
321 cross-sections. The two observed failure modes are shown in Figure 11. All sections reached a similar
322 shear strength of 10 MPa, +/- 7%, indicating that contrary to the bending tests, the grade does not
323 influence the shear capacity. Note that despite S_G2_Cross failing in the butt joint, it still reached a
324 strength of 10.4 MPa. Further optimisation of the cross bands layering may improve the shear capacity
325 of the CHS.

326 In terms of shear capacities, the slender sections sustained shear forces up to 32 kN and the com-
327 pact ones up to 60.8 kN.

328 The average oven dry moisture content at the time of testing of the sections tested in shear is
329 reported in Table 2.

330 **4.4 Compressive tests**

331 The compressive stress-strain curves (σ - ε) of all sections are plotted in Figure 12. Two different
332 types of curves are observed resulting in two different failure modes. The compact sections showed
333 a large non-linear plastic behaviour, with the load reaching a plateau before gradually decreasing. A
334 portion of the section wall ultimately locally buckled in a compression type failure mode, as shown
335 in Figure 13 (a). This led to a sudden drop of the load with the section remaining in one single piece.
336 For the slender sections, a plastic behaviour usually started to develop but premature failure (i.e.
337 before the load reached a plateau as for the compact sections) suddenly occurred with the sections
338 bursting into (i) two half cross-sections, with the failure occurring in the butt joint, for S_G2_Cross
339 and (ii) six to seven strips for all remaining slender sections. The latter failure mode is shown in
340 Figure 13 (b) and was also observed in [13, 32] for formed wood profiles. The slender sections could
341 therefore not reach their potential full capacity and exhibited a failure mode which should be avoided
342 in structures.

343 The compressive capacities R_c and strength f_c for all tested sections are reported in Table 5. The
344 ratios of f_c to the average material compressive strength σ_{comp} of the two half cross-sections (reported
345 in Table 1) are also given in the table. Similar to the bending tests, the compressive strength increases
346 with the veneer MOE (grade). Interestingly, both slender and compact sections reached a capacity
347 higher, up to 20%, than the one of the average measured compressive strength of the material. This
348 observation is in contradiction with the length effect [33, 34] encountered in timber structures for
349 which the larger the tested volume, the lesser the capacity. The circular shape of the section may
350 delay the compression failure of the cell walls when compared to the results reported in Section 4.1
351 and performed on flat panels. Further investigations are needed to validate and understand the ob-
352 served phenomena.

353 The compressive capacity is high for both section types and reached about 400-500 kN for the
354 slender sections to about 800-1,000 kN for the compact ones. For the compact sections, the capacity
355 is in the range of the design load which may be encountered in the columns of mid-rise timber build-
356 ings.

357 Also given in Table 5 are the static MOE E_s of the sections measured from the linear part of the
358 stress-strain curves (σ - ε) and the ratios of E_s measured from the bending tests to the one measured
359 from the compressive tests. The values of E_s measured from the two types of tests are consistent with
360 an average difference between the two values of 4%.

361 **4.5 Comparisons**

362 The structural efficiency of the compact sections is compared herein to the one of steel and rein-
363 forced concrete circular sections of similar (i) diameter and (ii) compressive short-term capacity to
364 the middle grade section C_G2 reported in Table 5. In a first instance only the short-term capacities
365 of the timber section is compared to the ultimate capacities of the steel and concrete counterparts,
366 which are calculated based on relevant Australian standards and without the use of the capacity factor
367 (resistance factor). Effect on long-term loading on the structural efficiency is discussed in a second
368 instance.

369 **4.5.1 Comparison to steel CHS**

370 A 168.3 (OD) \times 4.8 (wall thickness) CHS, commercialised by the Australian manufacturer
371 Onesteel [35], is selected for the structural steel section. Its yield stress is 350 MPa. Based on the
372 Australian and New-Zeeland standard AS4100 [36], the steel section has ultimate bending, shear and
373 compressive section capacities of $M_b = 44.8$ kN.m, $V_s = 311.2$ kN and $R_c = 864.5$ kN, respectively.
374 Its compressive capacity is within 4% of the one of C_G2.

375 Table 6 compares the ultimate capacities, ultimate capacity to linear weight ratios, bending and
376 axial stiffness of the steel and timber sections. Densities of 805 kg/m^3 for early to mid-rotation Gym-
377 pie messmate veneers [37] and $7,850 \text{ kg/m}^3$ for steel are used in Table 6. MOE of 200 GPa is also
378 used for the steel in the Table.

379 Results show that the timber CHS has a short-term bending capacity M_b comparable to and only
380 13% lower than the one of the steel CHS. Yet, the timber CHS is nearly twice more efficient in terms
381 of ultimate capacity to linear weight ratio. A similar conclusion applies to the compressive capacity
382 to linear weight ratio, with the timber section being more than twice more efficient than the steel
383 CHS. However, the steel CHS is stiffer than the timber profile, with the bending and axial stiffness
384 being 2.7 and 2.1 times higher, respectively.

385 Regarding the shear, the timber CHS performs poorly when compared to the steel profile. The
386 shear capacity V_s and shear to linear weight ratio of the steel CHS are 5.1 and 2.4 times higher, re-
387 spectively, than the ones of the timber sections. However, for the sizes of timber beams typically
388 encountered in structural applications, i.e. with a span to depth ratio of 20 [38], the shear capacity of
389 the timber section would be high enough. A simply supported, 3.5 m long, 167×25 timber CHS loaded
390 with a UDL which fails at an ultimate bending moment of 39.1 kN.m (C_G2 in Table 3), would
391 experience a maximum shear force of 44.7 kN. This shear force is 26% lower than the shear capacity
392 recorded for C_G2 in Table 4.

393 For long-term loading, the Australian standard AS1720.1 [39] uses a duration of load factor of
394 0.57. Therefore, using the same 168.3×4.8 steel CHS and comparing it to the timber CHS, but under
395 long-term loading, the timber section becomes 1.08 and 1.28 times more efficient than the steel CHS
396 in term of bending capacity to linear weight ratio and compressive capacity to linear weight ratio,
397 respectively. In terms of shear capacity to linear weight ratio, the timber CHS now becomes 4.16
398 times less efficient than the steel CHS.

399 4.5.2 *Comparison to reinforced concrete plain circular section*

400 A 167 mm diameter plain reinforced concrete column, with a concrete compressive strength $f'_c =$
401 40 MPa and a steel yield stress $f_y = 500$ MPa, was designed to standard practices and the Australian
402 Standard AS3600 [40]. While it is understood that a 167 mm diameter concrete columns would usu-
403 ally not be used in practice, it still forms a comparative solution to the performance of the timber
404 section. The concrete section is shown in Figure 14, has four N12 longitudinal reinforcing bars and
405 an R10 helix with a pitch of 150 mm. Based on the requirements in [40], a minimum concrete cover
406 of 20 mm is used with a minimum of 2% reinforcing steel by gross cross-sectional area. The AS3600
407 [40] gives ultimate bending, shear and compressive capacities of $M_b = 11.9$ kN.m, $V_s = 92$ kN and R_c
408 $= 946.4$ kN, respectively, for the concrete section. The compressive capacity of this column is there-
409 fore within 6% of the one of C_G2.

410 Table 6 compares the ultimate capacities, ultimate capacity to linear weight ratios, bending and
411 axial stiffness of the concrete and timber sections. The density of concrete for the calculations pre-
412 sented is $2,400$ kg/m³ and the MOE is $32,8$ GPa, in accordance to [40].

413 The ultimate bending capacity of the concrete section is significantly lower (3.3 times lower) than
414 the short-term bending capacity of the timber section. This results in the timber section being 22 times
415 more efficient than the concrete one in terms of bending capacity to linear weight ratio. On the other
416 hand, the bending stiffness of the concrete section is twice higher than the proposed timber section
417 and nearly as stiff as the steel section. Note that the small diameter of the concrete column results in
418 the steel being placed close to the neutral axis and therefore an inefficiency in resisting bending mo-
419 ments is introduced. It is anticipated that for columns of larger diameter, the efficiency of the concrete
420 column for these comparisons would improve.

421 In terms of shear, the shear capacity of the reinforced concrete section is 1.5 higher than the short-
422 term shear capacity of the timber section, yet the concrete solution is 3.9 less efficient than the timber
423 one in terms of shear capacity to linear weight ratio.

424 The concrete section is also the least efficient option in terms of compressive capacity to linear
425 weight ratio. It is 5.6 times and 2.5 less efficient than its timber and steel counterparts, respectively.
426 Nevertheless, it outperformed both the steel (1.5 times higher) and timber (3 times higher) solutions
427 in terms of compressive stiffness.

428 Regarding long-term loading and considering a duration of load factor of 0.57 [39] on the results
429 in Table 6, the concrete section becomes 12.5, 2.2 and 3.2 times less efficient in terms of bending,
430 shear and compressive capacity to linear weight ratios, respectively, when compared to the long-term
431 loading capacities of the timber section.

432

433 **5. CONCLUSION**

434 This paper presented the bending, shear and compression capacities, and structural behaviour, of
435 hardwood veneer-based CHS manufactured from early to mid-rotation (juvenile) Gympie messmate
436 plantation thinned logs. Twelve 167 mm (OD) \times 12.5 mm (wall thickness), referred to as “slender”,
437 and nine 167 mm (OD) \times 25 mm (wall thickness), referred to as “compact”, 1.2 m long CHS were
438 produced in seven sets of three nominally identical sections. The sections were tested in bending,
439 shear and compression. A sudden failure mode was observed in the compression zone of the slender
440 sections tested in bending, while the compact sections failed in the tension zone. The section had
441 shear capacities of the same order of magnitude, within 7% of each other. In compression, the com-
442 pact sections showed a ductile behaviour, while the slender sections catastrophically failed, with the
443 sections bursting into six to seven longitudinal strips. The section compressive strength was observed
444 to be consistently higher than the compressive strength of the material determined from tests per-
445 formed of flat samples. Comparison to steel and concrete sections of similar outside diameter proved
446 that the timber sections were the most efficient in terms of bending and compressive capacity to linear
447 weight ratio. However, while the timber sections fell behind their steel and concrete counterparts in

448 terms of shear efficiency, they still showed enough shear capacity for structural applications. The
449 optimisation of the cross-banded layering may improve the shear capacity without significantly im-
450 pacting the critical structural performances of the CHS.

451

452 **6. ACKNOWLEDGMENTS**

453 The authors would like to thank the *Australian Research Council* for its financial contribution
454 under project DE140100212. Mr Alexander Mainey glued the timber hollow sections. Mr Maxime
455 Fischer and Mr Julien Husson are also acknowledged for their valuable contribution in preparing the
456 hollow sections for testing and assisting during the tests.

457

458 **REFERENCES**

459

460 [1] B.P. Gilbert, I.D. Underhill, H. Bailleres, A. El Hanandeh, R.L. McGavin "Veneer Based
461 Composite hollow utility poles manufactured from hardwood plantation thinned trees", *Construction*
462 *and Building Materials*, 66, 458-466, 2014.

463 [2] B.P. Gilbert, I.D. Underhill, D. Fernando, H. Bailleres "Structural solutions to produce long timber
464 Veneer Based Composite hollow sections", *Construction and Building Materials*, 139, 81-92, 2017.

465 [3] I.D. Underhill, *The development and assessment of engineered wood products manufactured from*
466 *low grade eucalyptus plantation thinnings*, PhD Thesis, Griffith University, Gold Coast, Australia,
467 2017.

468 [4] H. Lu, A. El Hanandeh "Life cycle assessment of ACQ-treated Veneer Based Composite (VBC)
469 hollow utility poles from hardwood plantation mid-thinning", *Sustainable Production and*
470 *Consumption*, 36–50, 2016.

471 [5] H.R. Lu, A. El Hanandeh, B.P. Gilbert "A comparative life cycle study of alternative materials
472 for Australian multi-storey apartment building frame constructions: Environmental and economic
473 perspective", *Journal of Cleaner Production*, 166, 458-473, 2017.

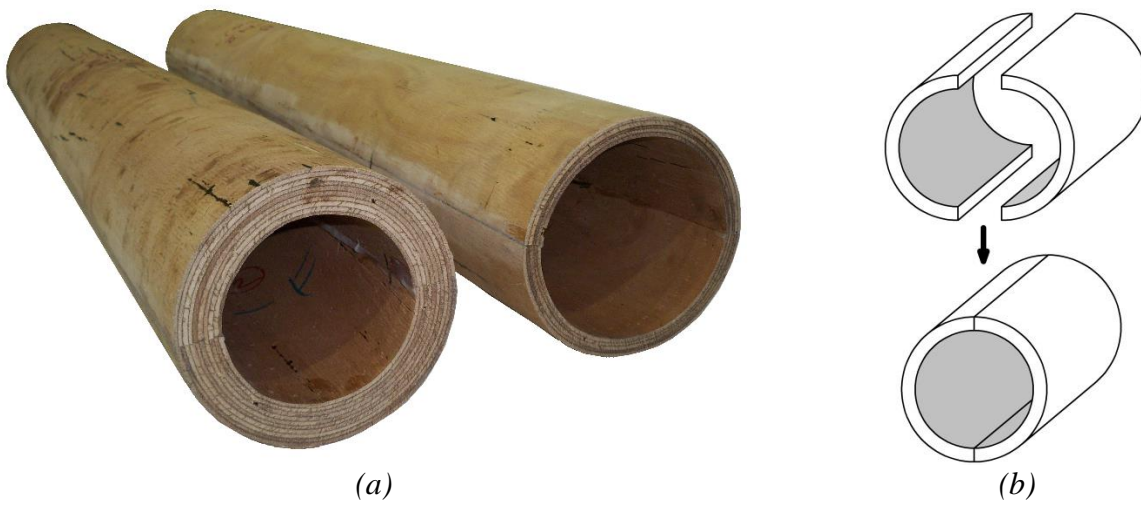
474 [6] H.R. Lu, A. El Hanandeh "Environmental and economic assessment of utility poles using life
475 cycle approach", *Clean Technologies and Environmental Policy*, 19, 1047-1066, 2017.

476 [7] T. Hata, K. Umemura, H. Yamauchi, A. Nakayama, S. Kawai, H. Sasaki "Design and pilot
477 production of a spiral-winder for the manufacture of cylindrical laminated veneer lumber", *Journal*
478 *of Wood Science*, 47, 115-123, 2001.

- 479 [8] P. Berard, P. Yang, H. Yamauchi, K. Umemura, S. Kawai "Modeling of a cylindrical laminated
480 veneer lumber I: mechanical properties of hinoki (*Chamaecyparis obtusa*) and the reliability of a
481 nonlinear finite elements model of a four-point bending test", *Journal of Wood Science*, 1-7, 2011.
- 482 [9] P. Berard, P. Yang, H. Yamauchi, K. Umemura, S. Kawai "Modeling of a cylindrical laminated
483 veneer lumber II: a nonlinear finite element model to improve the quality of the butt joint", *Journal*
484 *of Wood Science*, 1-7, 2011.
- 485 [10] J. Wehsener, T. Werner, J. Hartig, P. Haller, "Advancements for the structural application of
486 fiber-reinforced moulded wooden tubes", *Proceedings of the RILEM Conference "Materials and*
487 *Joints in Timber Structures - Recent Advancement of Technology"* (Eds.: S. Aicher, H.-W. Reinhardt,
488 H. Garrecht), Stuttgart, Germany, 99-108, 2013.
- 489 [11] P. Haller, J. Hartig, J. Wehsener, "Application of moulded wooden tubes as structural elements",
490 *Proceedings of the 2014 World Conference on Timber Engineering* (Ed.: A. Salenikovich), Quebec
491 City, Canada, Paper ABS684, 2014.
- 492 [12] L. Wang, W. Liu, D. Hui "Compression strength of hollow sandwich columns with GFRP skins
493 and a paulownia wood core", *Composites Part B: Engineering*, 60, 495-506, 2014.
- 494 [13] J.U. Hartig, J. Wehsener, P. Haller "Experimental and theoretical investigations on moulded
495 wooden tubes made of beech (*Fagus sylvatica* L.)", *Construction and Building Materials*, 126, 527-
496 536, 2016.
- 497 [14] A. Heiduschke, P. Haller "Fiber-Reinforced Plastic-Confined Wood Profiles Under Axial
498 Compression", *Structural Engineering International*, 20, 246-253, 2010.
- 499 [15] R.D. Adams, G.P. Krueger, A.E. Lund, D.D. Nicholas, "Development of utility poles from
500 composite wood material", *Proceedings of the 7th IEEE/PES Transmission and Distribution*
501 *Conference and Exposition* (Ed.: IEEE Service center), Atlanta, U.S.A., 37-40, 1979.
- 502 [16] C. Piao, *Wood laminated composite poles*, PhD Thesis, School of renewable natural resources,
503 Louisiana State University, Louisiana, U.S.A., 2003.
- 504 [17] N.Ç. Yerlikaya, A. Aktaş "Compressive failure of spruce wood rings reinforced with glass epoxy
505 composite", *Journal of Forestry Research*, 26, 517-522, 2015.
- 506 [18] S. Hirschmüller, J. Pravida, R. Marte, M. Flach "Long-term material properties of circular hollow
507 laminated veneer lumber sections under water saturation and cement alkaline attack", *Wood Material*
508 *Science & Engineering*, 1-15, 2018.
- 509 [19] Lignotube, *LignoTUBE – the new semi-finished product for lightweight construction*,
510 <http://lignotube.com/description/>, 2017
- 511 [20] K+W Formholztechnik GmbH, *Rings and Tubes*,
512 http://www.formholz.de/produkte_und_loesungen/standardprodukte/ringe_und_roehren, 2017
- 513 [21] J. Bond, Foundations of tree risk analysis: Use of the t/R ratio to evaluate trunk failure potential,
514 in: *Arborist news*, December 2006, pp. 31-34.

- 515 [22] A.H. Buchanan "Bending Strength of Lumber", *ASCE Journal of Structural Engineering*, 116,
516 1213-1229, 1990.
- 517 [23] L.G. Brazier "On the Flexure of Thin Cylindrical Shells and Other "Thin" Sections", *Proceedings*
518 *of The Royal Society*, 116, 104-116, 1927.
- 519 [24] L. Brancheriau, H. Bailleres "Natural vibration analysis of clear wooden beams: a theoretical
520 review", *Wood Science and Technology*, 36, 347–365, 2002.
- 521 [25] CIRAD, *BING® (Beam Identification by Nondestructive Grading) software*,
522 <https://www.picotech.com/library/application-note/non-destructive-testing-of-wood>, 2012
- 523 [26] I.D. Underhill, B.P. Gilbert, H. Bailleres, R.L. McGavin, D. Patterson, "Structural Veneer Based
524 Composite products from hardwood thinning – Part I: Background and manufacturing", *Proceedings*
525 *of the RILEM Conference "Materials and Joints in Timber Structures - Recent Advancement of*
526 *Technology"* (Eds.: A. Aicher, H.-W. Reinhardt, H. Garrecht), Stuttgart, Germany, 577-588, 2013.
- 527 [27] S. Hirschmüller, J. Pravida, R. Marte, "Laminated veneer lumber poles for temporary soil
528 nailing- investigation of material properties", *Proceedings of the 2016 World Conference on Timber*
529 *Engineering* (Eds.: J. Eberhardsteiner, W. Winter, A. Fadai, M. Pöll), Vienna, Austria, Electronic
530 proceedings, 2016.
- 531 [28] AS/NZS 1080.1, *Timber - Methods of test - Moisture content*, Standards Australia, Sydney,
532 Australia, 2012.
- 533 [29] ASTM D3500-14, *Standard Test Methods for Structural Panels in Tension*, ASTM International,
534 Pennsylvania, USA, 2014.
- 535 [30] J. Wardenier, *Hollow timber sections in structural applications*, (Comité International pour le
536 Développement et l'Etude de la Construction Tubulaire), 2001.
- 537 [31] B.P. Gilbert, H. Bailleres, M.F. Fischer, H. Zhang, R.L. McGavin "Mechanical properties of
538 rotary veneers recovered from early to midrotation subtropical-hardwood plantation logs for veneer-
539 based composite applications.", *ASCE Journal of Materials in Civil Engineering*, 29, 04017194,
540 2017.
- 541 [32] A. Heiduschke, J.M. Cabreo, C. Manthey, P. Haller, E. Gunther, "Mechanical behaviour and life
542 cycle assessment of fibre-reinforced timber profiles", *Proceedings of the Sustainability of*
543 *Constructions - Integrated approach to lifetime engineering* (Ed.: COST Action C25), 338-346, 2008.
- 544 [33] J.D. Barrett, F. Lam, W. Lau "Size Effects in Visually Graded Softwood Structural Lumber",
545 *ASCE Journal of Materials in Civil Engineering*, 7, 19-30, 1995.
- 546 [34] B. Madsen "Length effects in 38 mm spruce–pine–fir dimension lumber", *Canadian Journal of*
547 *Civil Engineering*, 17, 226-237, 1990.
- 548 [35] Australian Tube Mills, Design Capacity Tables for Structural Steel Hollow Sections, Australian
549 Tube Mills Pty Ltd., Sunnybank, Australia, 2013.
- 550 [36] AS 4100, *Steel structures* Standards Australia, Sydney, Australia, 1998.

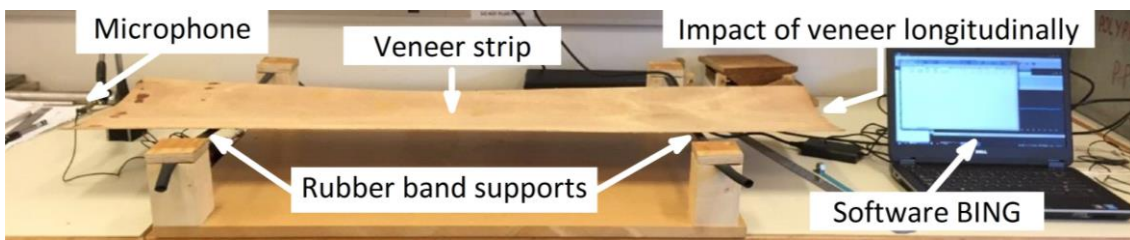
- 551 [37] R.L. McGavin, H. Bailleres, J. Fehrmann, B. Ozarska "Stiffness and Density Analysis of Rotary
552 Veneer Recovered from Six Species of Australian Plantation Hardwoods", *BioResources*, 10, 6395-
553 6416, 2015.
- 554 [38] D.L. Schodek, *Structures - 2nd Edition*, (Prentice-Hall), 1992.
- 555 [39] AS 1720.1, *Timber structures, Part 1: Design methods*, Standards Australia, Sydney, Australia,
556 2010.
- 557 [40] AS 3600, *Concrete structures*, Standards Australia, Sydney, Australia, 2009.
558
559



560
561

562 **Figure 1:** (a) circular hollow section currently developed in Australia (shown for compact and
563 slender 167 mm (OD) Gympie messmate) and (b) principle of half cross-sections butt joined to-
564 gether to form a complete CHS

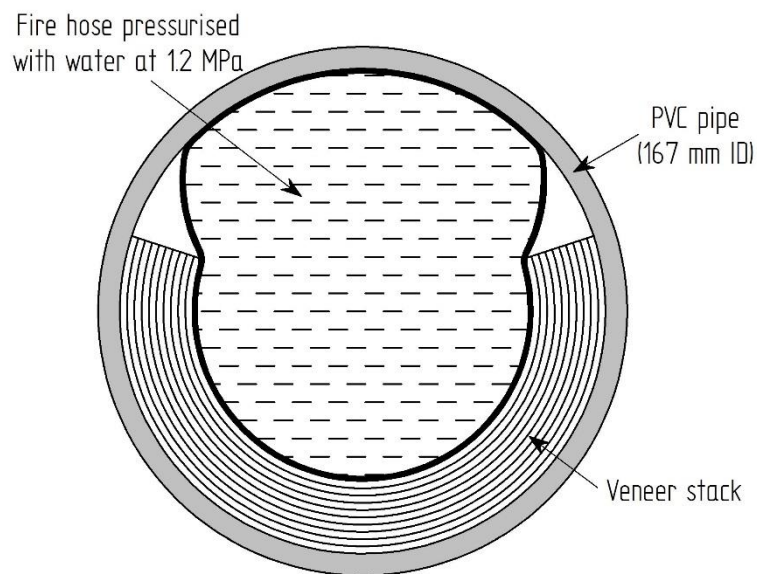
565



566
567

Figure 2: Set-up to assess the longitudinal MOE

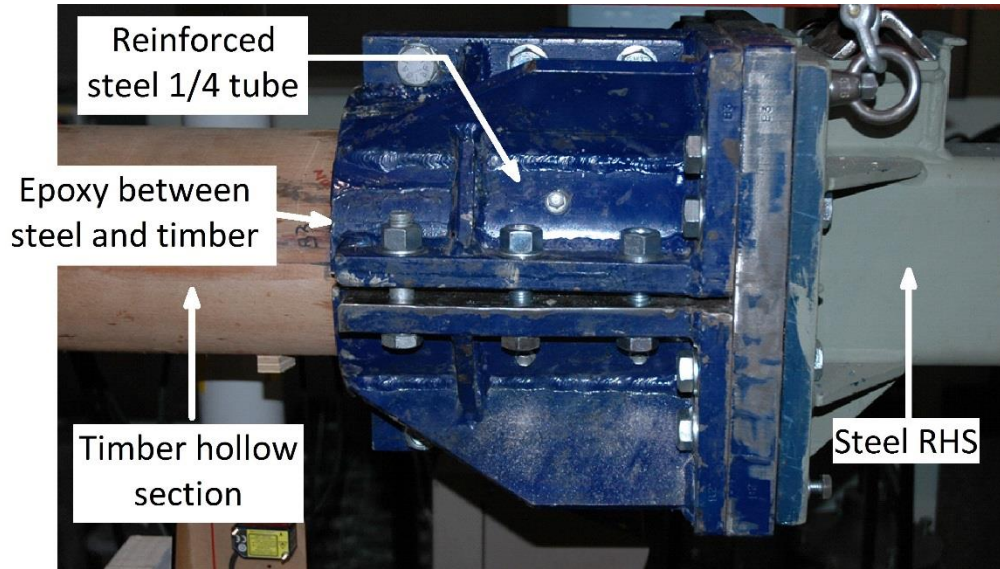
568



569
570

Figure 3: Manufacturing process of the half cross-sections

571



572

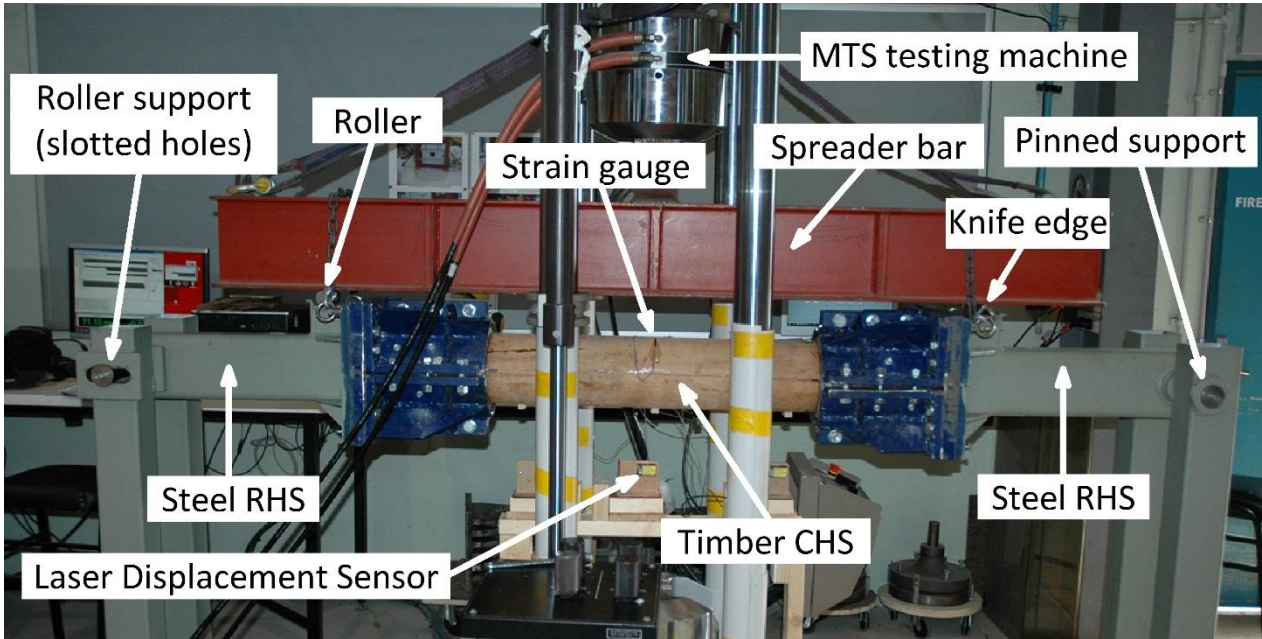
573

Figure 4: Clamps to connect timber CHS to test rig

574

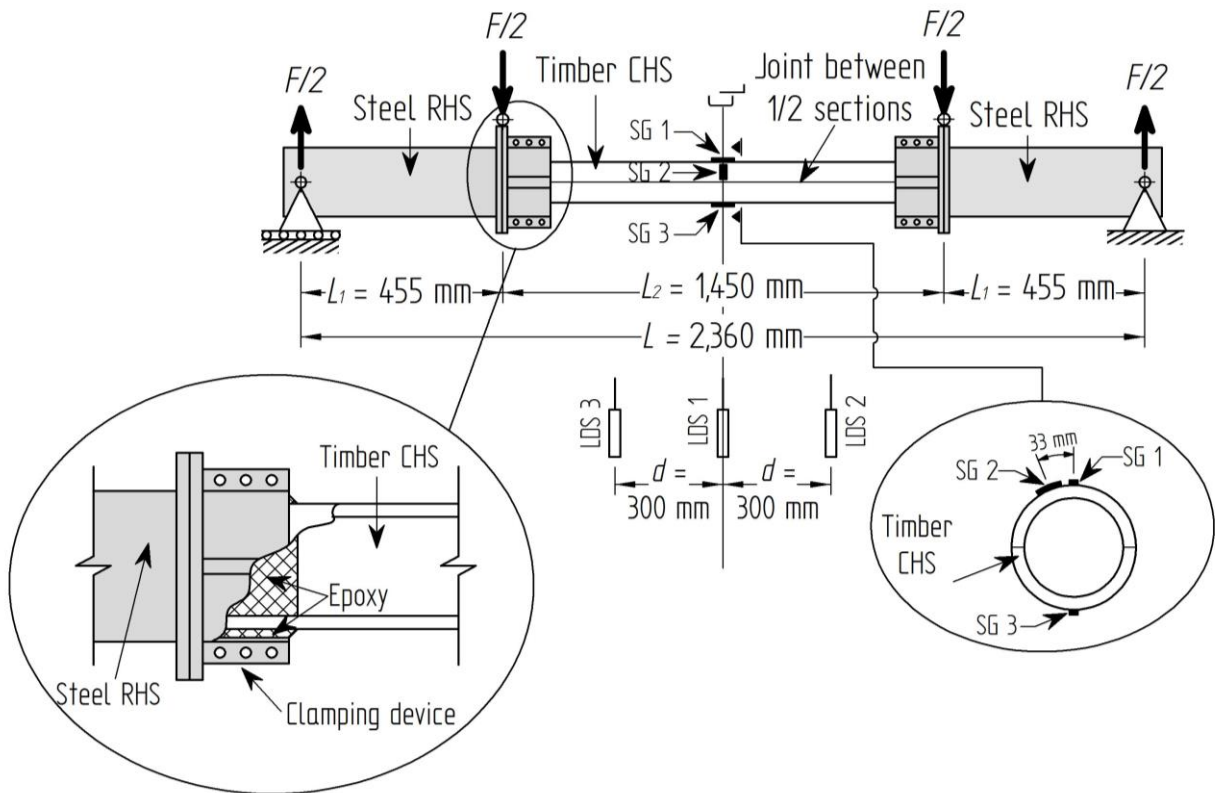
575

576



577
578

(a)



(b)

579
580

581

Figure 5: Bending test set-up, (a) overall picture and (b) schematic

582

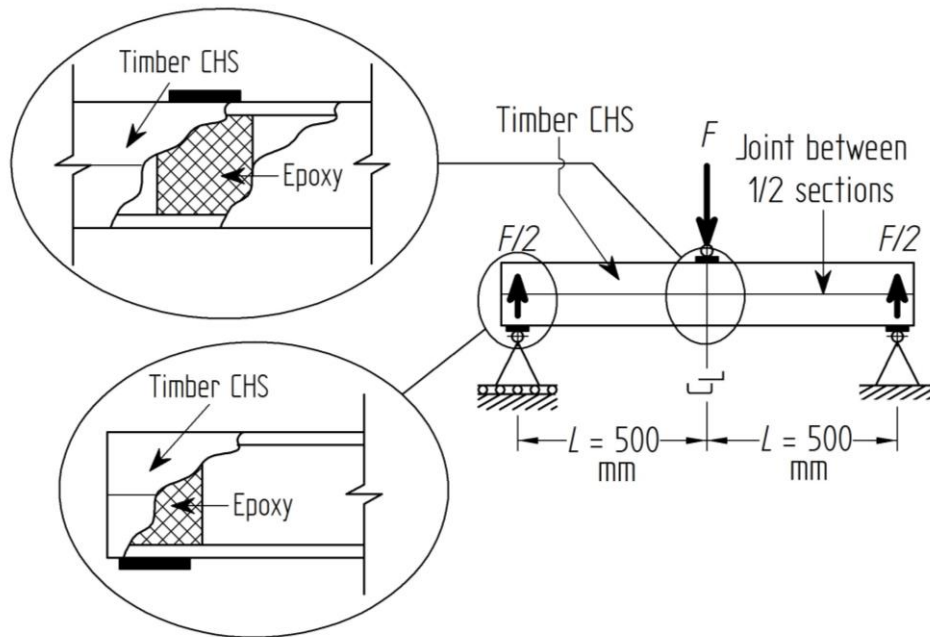


Figure 6: Shear test set-up

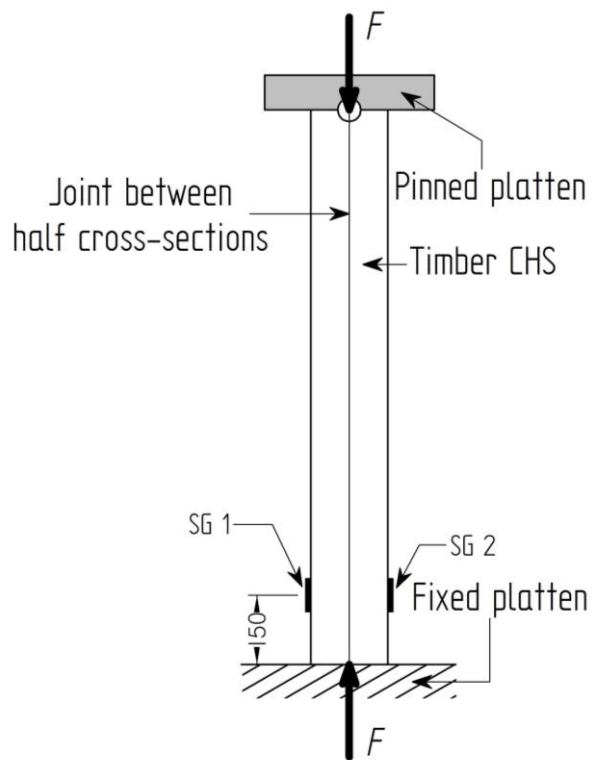


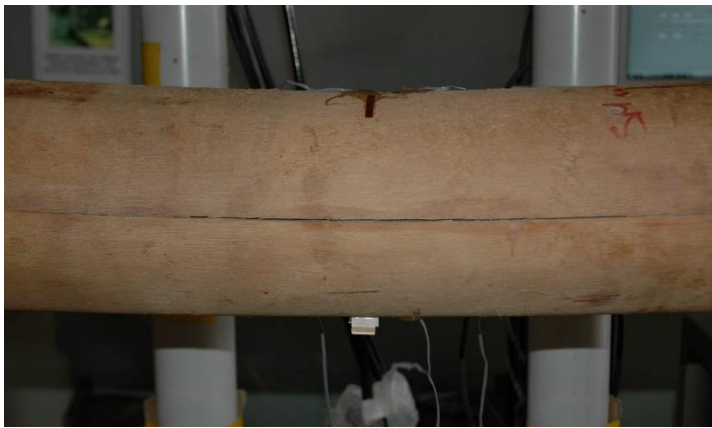
Figure 7: Compression test set-up



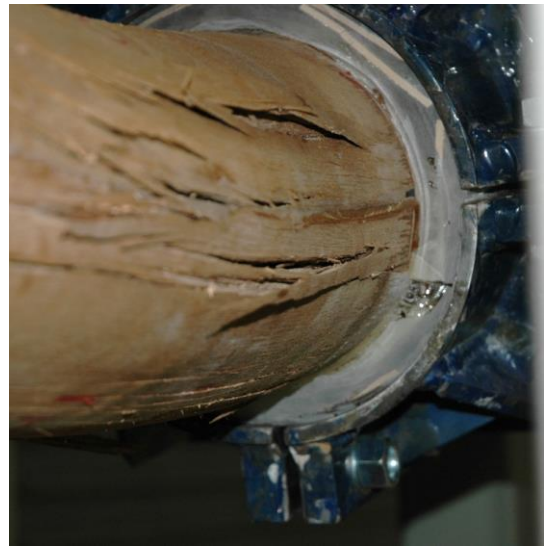
(a)



(b)



(c)



(d)

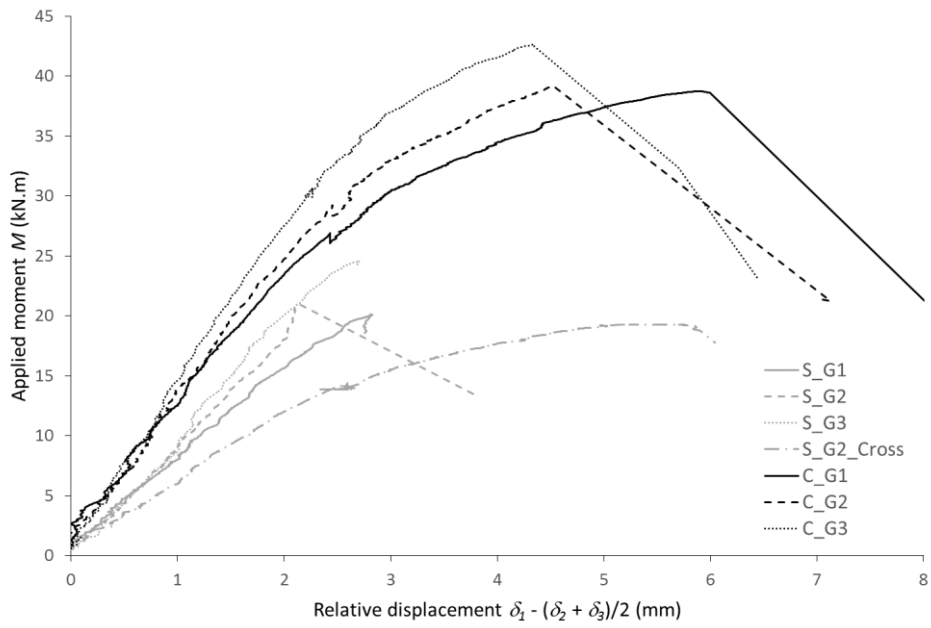
589
590
591

592
593

594 **Figure 8:** Bending tests failure modes (a) buckling of the compression zone (shown for S_G3), (b)
595 Tensile rupture (shown for C_G1), (c) initial failure in the butt joint for C_G2_Cross and (d) prem-
596 ature failure at the steel-timber connections (shown for C_G2)

597

598



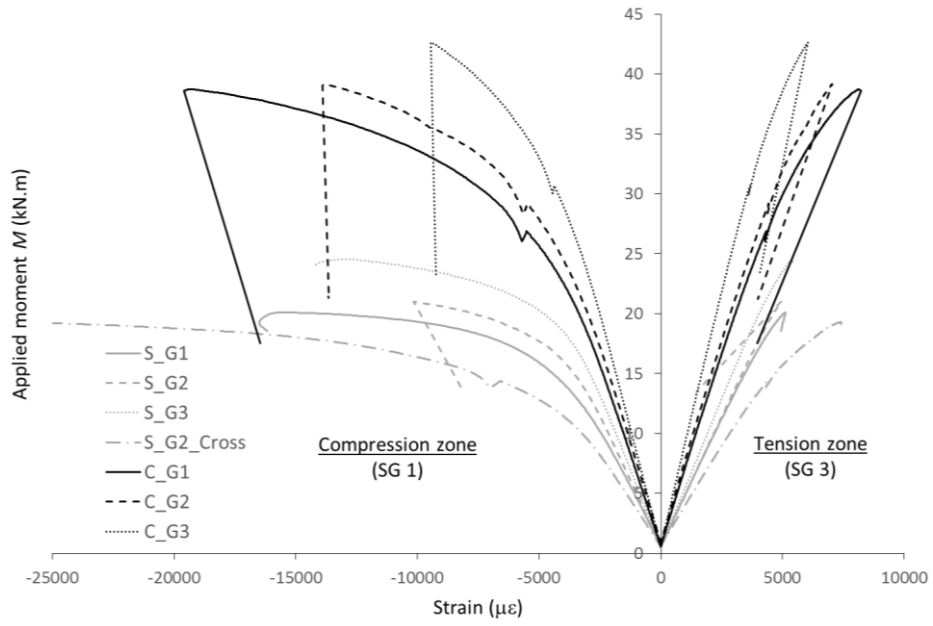
599

600

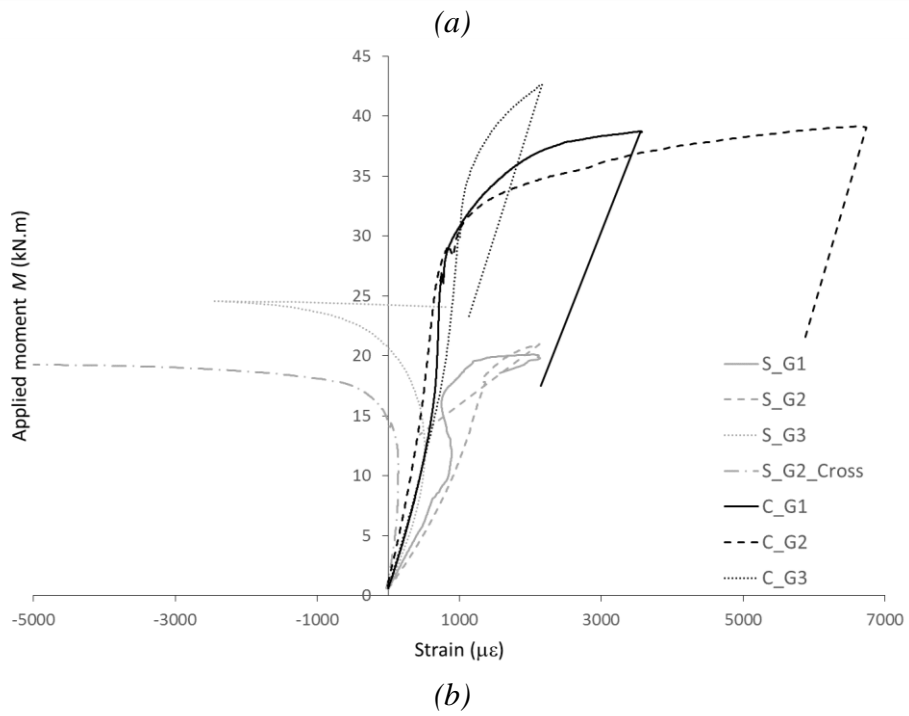
Figure 9: Bending tests, Moment-Displacement curves ($M-\delta$) for all investigated sections

601

602



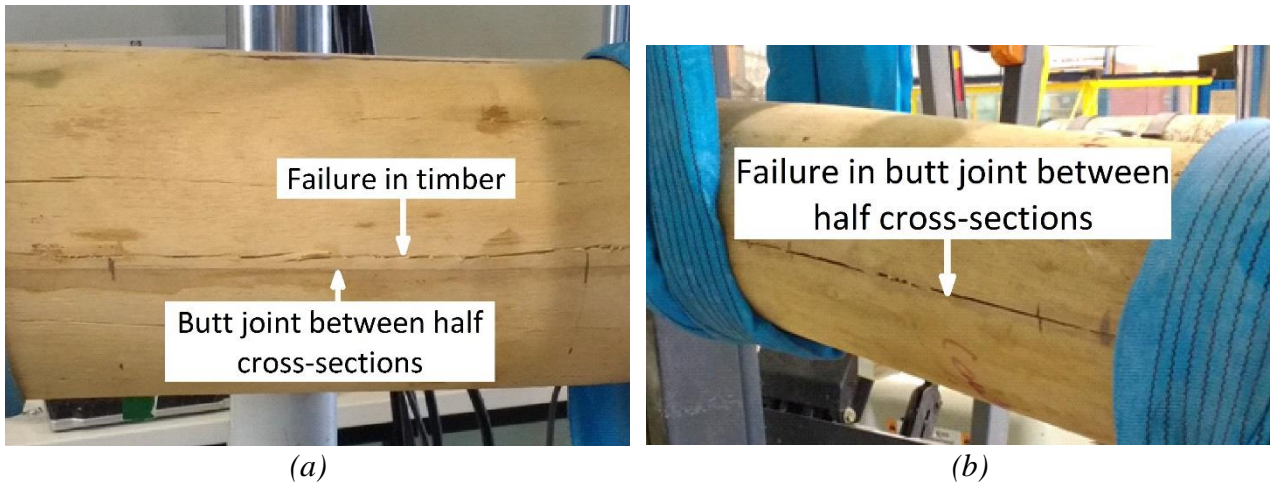
603
604



605
606

607 **Figure 10:** Bending tests, Strain gauge readings for all investigated sections (a) longitudinal strain
608 gauges (SG 1 and SG 3) and (b) transverse strain gauge (SG 2)

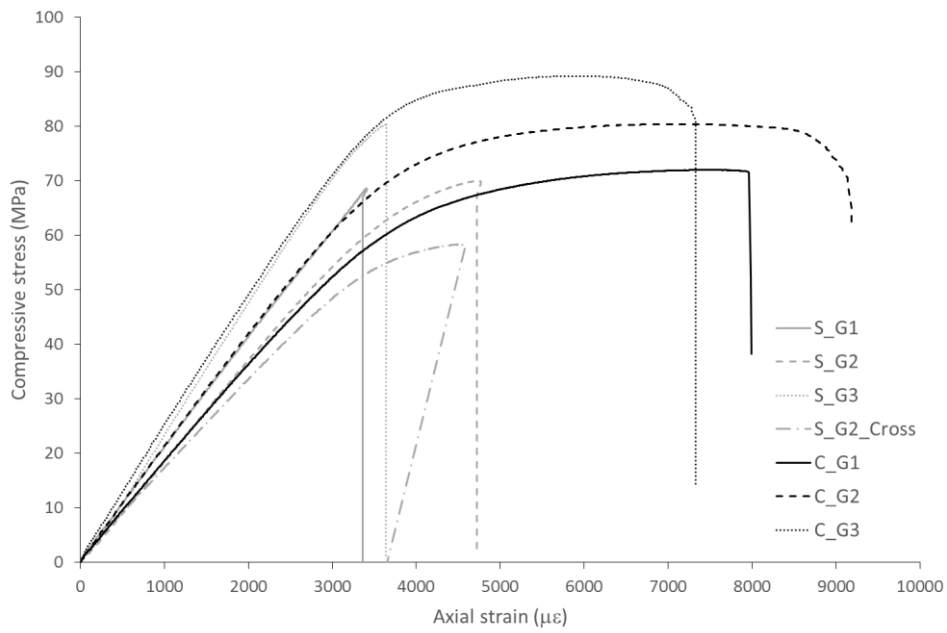
609



610
611

612 **Figure 11:** Shear tests failure modes (a) failure in the timber for all sections but C_G2_Cross
613 (shown for S_G3) and (b) failure in the butt joint for C_G2_Cross

614



615

616 **Figure 12:** Compression tests, Stress-Strain curves (σ - ϵ) of all investigated sections

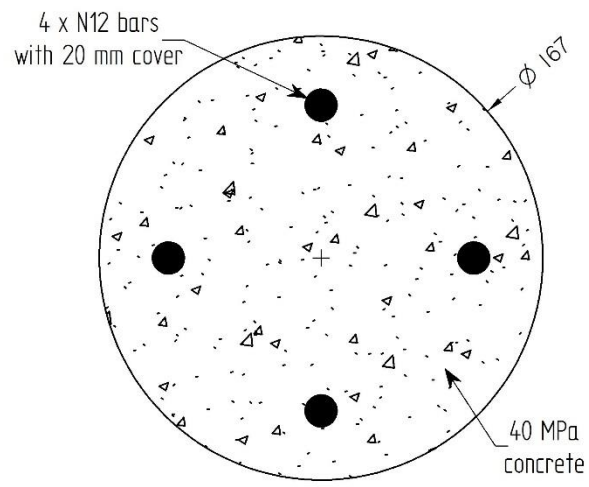
617



618
619

620 **Figure 13:** Compression tests failure modes, (a) local buckling of the wall for the compact sections
621 (shown for C_G1) and (b) sudden failure with the sections bursting into strips for the slender sec-
622 tions with no cross-banded veneers (shown for S_G2)

623



624

625

Figure 14: Concrete section used for comparison purposes

626

627
628

629 **Table 1:** Average compressive and tensile strengths of the material (numbers in brackets indicate
630 the number of tests on which the average and Coefficient of Variation (CoV) are calculated)

Set	Half cross-section 1 ⁽¹⁾				Half cross-section 2 ⁽¹⁾			
	σ_{comp} (MPa)	CoV (%)	σ_{tens} (MPa)	CoV (%)	σ_{comp} (MPa)	CoV (%)	σ_{tens} (MPa)	CoV (%)
S_G1	61.2 (3)	4.2	109.5 (5)	21.4	58.6 (3)	<0.1	96.7 (3)	7.3
S_G2	65.5 (3)	5.3	101.0 (4)	31.1	69.2 (3)	3.5	119.1 (5)	11.4
S_G3	72.7 (3)	3.2	114.0 (5)	31.9	77.9 (3)	3.4	-- ⁽²⁾	-- ⁽²⁾
S_G2_Cross ⁽³⁾	54.0 (3)	0.5	94.4 (5)	5.3	59.9 (2)	12.3	88.9 (5)	15.7
C_G1	67.0 (2)	1.9	99.3 (5)	6.9	64.4 (4)	3.4	96.3 (5)	7.7
C_G2	67.8 (2)	7.2	117.2 (5)	8.7	66.7 (4)	1.6	134.0 (5)	11.8
C_G3	77.9 (2)	3.6	133.0 (5)	8.8	71.3 (3)	2.4	135.8 (5)	11.5

631 ⁽¹⁾: Half cross-section #1 in tension and half cross-section #2 in compression during the bending and shear tests

632 ⁽²⁾: Samples lost by the external company which CNC cut the samples

633 ⁽³⁾: Strengths calculated using the gross measured cross-sectional area which includes cross-banded veneers

634

635 **Table 2:** Average measured moisture content (MC) for material testing and full cross-sections
636 (numbers in brackets indicate the number of samples on which the average and Coefficient of Vari-
637 ation (CoV) are calculated)

Sample type	Test type	MC (%)	CoV (%)
Material testing	Compression	13.7 (10)	3.4
	Tension	11.3 (14)	5.7
Full cross-sections	Bending	13.7 (4)	4.2
	Shear	12.2 (4)	1.9

638

639 **Table 3:** Bending tests results

Set	Capacity M_b (kN.m)	Strength f_b (MPa)	MOE E_s (MPa)	Failure mode
S_G1	20.1	96.9	20154	Compression (buckling) failure
S_G2	21.0	96.3	23252	Tension failure
S_G3	24.6	116.7	27883	Compression (buckling) failure
S_G2_Cross ⁽¹⁾	19.3	88.5	14947	Failure in joint between 1/2 cross-sections
C_G1	38.7	116.1	18590	Tension failure
C_G2	39.1	119.0	21666	Failure at support with steel clamps
C_G3	42.6	128.6	23331	Failure at support with steel clamps

640 ⁽¹⁾: Strength f_b calculated using the gross measured cross-section which includes cross-banded veneers

641

642

643

Table 4: Shear tests results

Set	Capacity V_s (kN)	Strength f_s (MPa)
S_G1	30.5	10.3
S_G2	29.5	9.5
S_G3	30.9	9.9
S_G2_Cross ⁽¹⁾	32.0	10.4
C_G1	53.9	9.5
C_G2	60.8	10.7
C_G3	58.5	10.6

644 ⁽¹⁾: Strength f_s calculated using the gross measured cross-section which includes cross-banded veneers

645

646

Table 5: Compression tests results

Set	Capacity R_c (kN)	Strength f_c (MPa)	MOE E_s (MPa)	Section strength $f_c /$ material strength σ_{comp}	E_s (bending) / E_s (compression)
S_G1	438.2	68.6	18824	1.15	1.07
S_G2	451.4	70.0	20592	1.04	1.13
S_G3	488.0	80.3	24709	1.07	1.13
S_G2_Cross ⁽¹⁾	372.3	58.4	16343	1.02	0.91
C_G1	784.0	72.0	17852	1.10	1.04
C_G2	897.8	80.4	20849	1.20	1.04
C_G3	992.4	89.3	24529	1.20	0.95

647 ⁽¹⁾: Strength f_c calculated using the gross measured cross-section which includes cross-banded veneers

648

649

Table 6: Structural efficiency of circular timber, steel and reinforced concrete sections

Section	Bending			Shear		Compression		
	M_b (kN.m)	$M_b /$ linear weight (kN.m/kg)	Stiffness EI (kN.m ²)	V_s (kN)	$V_s /$ linear weight (kN/kg)	R_c (kN)	$R_c /$ linear weight (kN/kg)	Stiffness EA (kN)
Timber (C_G2)	39.1	4.4	6.15×10^2	60.8	6.8	897.8	100.0	2.37×10^5
Steel (168×4.8)	44.8	2.3	1.65×10^3	311.2	16.1	864.5	44.6	4.94×10^5
Concrete	11.9	0.2	1.22×10^3	92.0	1.8	946.4	18.0	7.18×10^5

650